



# Fuzzy Controlled Isolated Micro-grid with Battery Storage and Renewable Energy Sources

Bairi Venkateshwarlu

Assistant Professor

Department of EEE

LORDS Inst. of Engg. & Tech, JNTUH

Email id: [bairivenkatesh@gmail.com](mailto:bairivenkatesh@gmail.com)

K Nookaraju

Assistant Professor

Department of EEE

LORDS Inst. of Engg. & Tech, JNTUH

Email: [raju2vizag@gmail.com](mailto:raju2vizag@gmail.com)

Koduri Rajender

M Tech Scholar

Department of EEE

LORDS Inst. of Engg. & Tech, JNTUH

Email: [koduri.rajender@gmail.com](mailto:koduri.rajender@gmail.com)

**Abstract-** The Proposed concept is implemented to fuzzy controlled. The enabling of ac micro grids in distribution networks allows delivering distributed power and providing grid support services during regular operation of the grid, as well as powering isolated islands in case of faults and contingencies, thus increasing the performance and reliability of the electrical system. This project proposes an alternative strategy to control the generated power within an isolated ac microgrid with distributed RES. The proposal is to control the terminal voltage of the existing battery banks below or equal its maximum allowable value. In this particular study, the power system consists of a power electronic converter supplied by a battery bank, which is used to form the ac grid (grid former converter), an energy source based on a wind turbine with its respective power electronic converter (grid supplier converter), and the power consumers (loads). The main objective of this proposed strategy is to control the state of charge of the battery bank limiting the voltage on its terminals by controlling the power generated by the energy sources. This is done without using dump loads or any physical communication among the power electronic converters or the individual energy source controllers. The electrical frequency of the micro grid is used to inform the power sources and their respective converters about the amount of power that they need to generate in order to maintain the battery-bank charging voltage below or equal its maximum allowable limit using mat lab/simulation link software

**Index Terms**—Battery banks, isolated micro grids, parallel inverters, power control, renewable energy sources (RESs), state of charge (SOC).

## I. INTRODUCTION

Micro grids are becoming popular in distribution systems because they can improve the power quality and reliability of power supplies and reduce the environmental impact. Micro grid operation can be classified into two modes: grid-connected and islanded modes. In general, micro grids are comprised of distributed energy resources (DERs) including renewable energy sources, distributed energy storage systems (ESSs), and local loads [1–3]. However, the use of renewable energy sources such as wind and solar power in micro grids causes power flow variations owing to uncertainties in their power outputs.

These variations should be reduced to meet power-quality requirements [4,5]. This study focuses on handling the problems that are introduced by wind power. To compensate for fluctuations in wind power, various ESSs have been implemented in micro grids. Short-term ESSs such as superconducting magnetic energy storage (SMES) systems [6], electrical double-layer capacitors (EDLCs) [7], and flywheel energy storage systems (FESSs) as well as long-term ESSs such as battery energy storage systems (BESSs) [8-9] are applied to micro grid control. ESSs can also be used to control the power flow at point of common coupling in the grid-connected mode as well as to regulate the frequency and voltage of a micro grid in the islanded mode. Among these ESSs, BESSs have been implemented widely owing to their versatility, high energy density, and efficiency. Moreover, their cost has decreased whereas their performance and lifetime has increased.

In practice, BESSs with high performance such as smooth and fast dynamic response during charging and discharging are required for microgrid control. This performance depends on the control performance of the power electronic converter. Proportional-integral (PI) control is a practical and popular control technique for BESS control systems. However, PI control might show unsatisfactory results for nonlinear and discontinuous systems [10].

When properly applied, these new, distributed generation units (DG) offer significant benefit to the grid and to end users. However, merging DGs into the traditional grid is not without technological challenges. The traditional electrical grid was not designed for power generation sources distributed near the ends of the T&D grid. The successful integration of DG power sources requires the single-direction grid architecture of the past transition to a smarter and more agile bi-directional grid [11]. As DGs continue to gain traction in the electrical market, new thinking and new strategies around power generation, distribution and consumption will continue to emerge. One of the increasingly common tactics for merging DGs

into the larger electrical grid is a new twist on an old electrical architecture known as the microgrid.

Micro grids are areas of the grid that can operate as part of the larger macro grid or operate autonomously as a standalone system. The micro grid systems help facilitate the integration of DG assets into the larger electrical grid. Further, when properly implemented, micro grids can unlock a wide array of stacked values for grid operators and electrical consumers [12].

## II. SYSTEM DESCRIPTION

Fig. 1 illustrates the simplified diagram of a stand-alone microgrid used to explain the control strategy proposed in this paper. It consists of a GFC, a GSC, and a battery bank. The renewable energy source, in this particular study, is a variable speed wind turbine coupled to a permanent-magnet synchronous generator (PMSG). Depending on the system size, other energy sources and other storage energy systems can be distributed along the microgrid. The simplicity of this system is useful to show the feasibility of the proposed control strategy without losing generality.

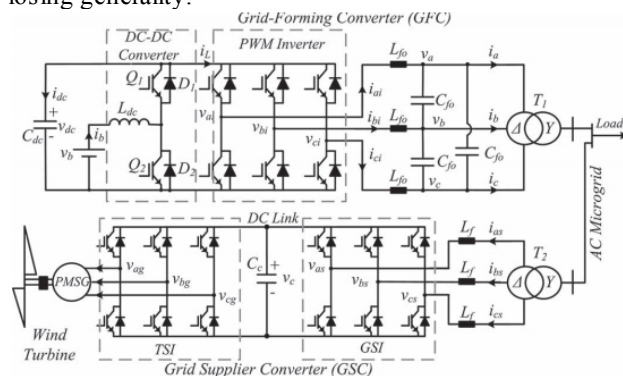


Fig. 1. Simplified diagram of the studied microgrid.

The GFC is a bidirectional converter formed by a pulse width modulation (PWM) three-phase inverter and a dc-dc converter that works in a buck mode when the battery bank is undercharge or in a boost mode when it is under discharge. The PWM inverter controls the magnitude and frequency of the microgrid

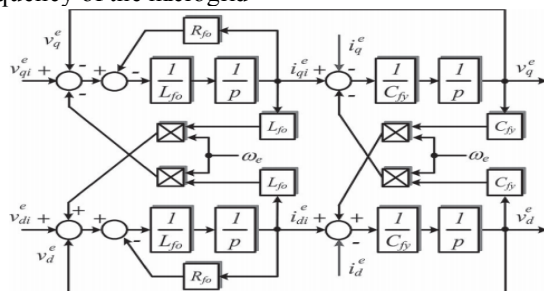


Fig. 2. Block diagram of LC filter implemented in a synchronous reference frame.

Voltage, while the dc-dc buck or boost converter is used to control the voltage at the dc bus capacitor ( $C_{dc}$ ) which is the dc bus voltage as well as the charging and discharging of the battery bank.

The GSC is used to control the power generated by the renewable energy source. In this particular example, the converter is formed by a conventional back-to-back topology [12]. It has a grid-side PWM inverter (GSI) and a wind turbine-side PWM inverter (TSI). The GSI is used to control the dc-link voltage of the back-to-back topology, and the TSI is used to control the power generated by the wind turbine based on a maximum power point tracker (MPPT) algorithm.

## III. GRID FORMER CONVERTER

### A. Control of the Microgrid Voltage and Frequency

The microgrid voltage controller uses the traditional configuration implemented on a synchronous dq reference frame, with an inner current loop and an outer voltage loop [7]. The frequency and voltage reference values are calculated using a droop control strategy as a function of the active and reactive powers, respectively, at the grid former converter terminals. The dq model of the LC filter in the delta side of transformer T1 (see Fig. 1) is used to design the control loops of the GFC. The block diagram of this model is shown in Fig. 3, where  $R_{f0}$  is the equivalent series resistance of the filter inductor  $L_{f0}$ ;  $\omega_e$  is the microgrid frequency in radians per second, the super script's "e" denotes variables in the dq synchronous reference frame,  $i_{ed}$  and  $i_{eq}$  are the dq currents in the delta side of transformer T1;  $C_{fy}$  is the per-phase equivalent capacitance of the LC filter and is equal to  $3C_{fo}$ ; and  $v_{qe}$  and  $v_{de}$  are the dq voltages in the capacitors of the LC filter. The subscript i denotes the output variables of the GFC PWM inverter. All the block diagrams shown in this paper use the operator  $p = d/dt$ . Based on the model presented in Fig. 2, an inner current loop and an outer voltage loop were designed, as illustrated in Fig. 3.

In this figure, "Λ" denotes estimated parameters, and  $G_{DID1}$  is the transfer function used to decouple at the sample instants the effect of the disturbances due to the load currents  $i_{eq}$ ,  $i_{ed}$  and the cross-coupling due to  $v_{qe}$  and  $v_{de}$ . ZOH means zero-order hold (latch).

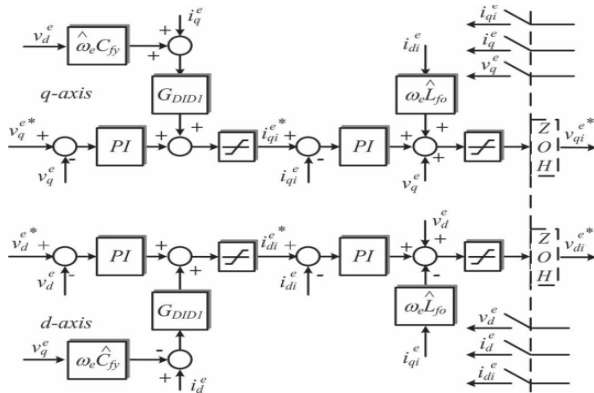


Fig. 3. Block diagram of the microgrid voltage controller.

Fundamentally, the current on the inductance  $L_f$  is controlled in order to regulate the voltage on the capacitance  $C_f$ , independently whether the power flux is from the PWM inverter to the microgrid or vice versa. The voltage reference values for the voltage controllers can be constant, generally equal to the nominal value of the microgrid voltage, or can be calculated based on a droop control strategy. In this paper, the voltage reference was fixed in 220 V (rms line voltage in the delta side of T1).

**B. Control of the Bidirectional DC-DC Converter**

The dc-dc converter (in GFC) is used to control the voltage in the capacitor  $C_{dc}$ . The action of the controller of the dc-dc converter can be considered equivalent to connecting an uncontrolled voltage source, with mean value  $V_{ct}$ , between the external terminals of the converter circuit, as shown in Fig. 4(a) and (b). If the losses in the converter are not considered, the voltage on  $C_{dc}$  depends only on the difference between the power at the battery bank terminals ( $P_b$ ) and ( $P_{inv}$ ) which is the power at the terminals of the delta side of the isolation transformer T1, which is positive when the power flux is from the inverter to the grid and negative on the contrary. This is shown in Fig. 4(c). Therefore, the dynamic equation for  $v_{dc}$  can be written as in (1), where  $w_{dc}$  is an auxiliary variable defined by  $w_{dc} = v_{dc}^2$

$$\frac{1}{2} C_{dc} \frac{dv_{dc}^2}{dt} = \frac{1}{2} C_{dc} \frac{dw_{dc}}{dt} = P_b - P_{inv} \quad (1)$$

From (1) and Fig. 4, the dc bus voltage controller of the GFC can be designed with an inner current loop to control the battery bank current ( $i_b$ ) and an outer voltage loop to control the voltage over the capacitor  $C_{dc}$ , as illustrated in Fig. 6.

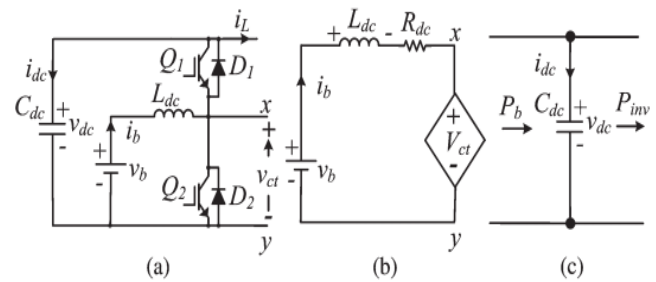


Fig. 4. DC-DC converter average model: (a) Original circuit, (b) equivalent average circuit of inductor and battery bank, and (c) average model of the bus dc.

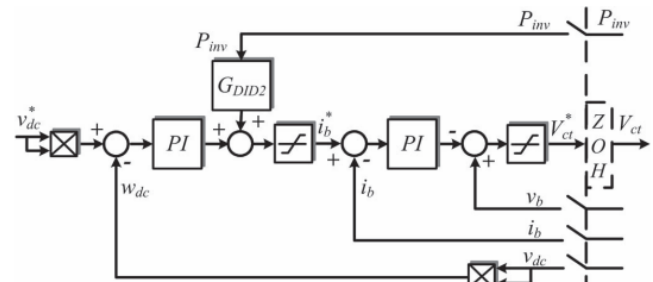


Fig. 5. Block diagram of the voltage controller of the dc-dc converter.

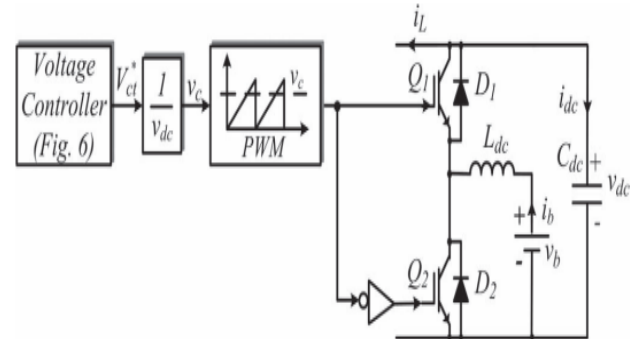


Fig. 6. Block diagram of the commands for the switches of the dc-dc converter.

GDID2 is used to decouple the power disturbance from the output of the inverter over the dc bus voltage. The output of the voltage controller ( $V_{ct}$ ) is the reference value for the PWM block used to generate the control signal for Q1 or Q2 switches, as shown in Fig. 6 [4]. In Fig. 6, when  $P_{inv}$  is positive, the battery bank supplies the load, and the dc-dc converter functions on the boost mode using the Q2 switch and D1 diode. On the other hand, when  $P_{inv}$  is negative, the dc-dc converter functions on the buck mode using the Q1 switch and D2 diode.

**IV. GRID SUPPLIER CONVERTER**

**A. Control of the Injected Current in the Microgrid and the Voltage at the DC Bus**

In this paper, the GSI of the GSC (see Fig. 1) is used to control the dc bus voltage of the back-to-back topology.

This controller uses an inner current loop to control the injected current in the microgrid. The current controller is implemented in a dq synchronous reference frame aligned with the microgrid positive sequence voltage vector. The converter variable synchronization is done by using a synchronous phase-locked loop (PLL) that has a second-order resonant filter tuned for the fundamental frequency of the microgrid.

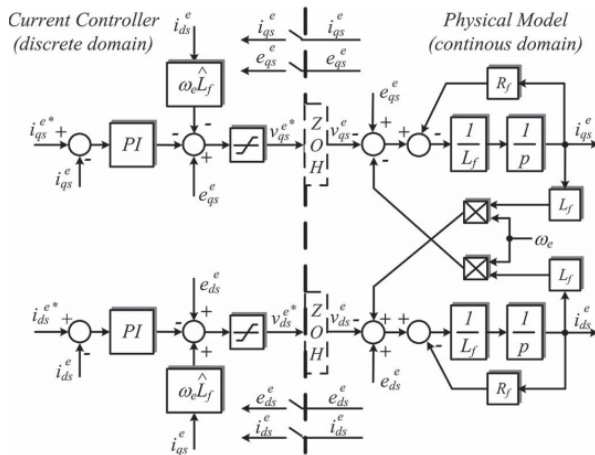


Fig. 7. Block diagram of the control of the injected current in the microgrid by the GSC.

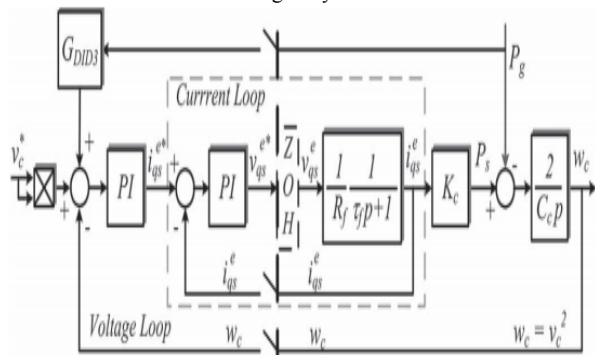


Fig. 8. Block diagram of the dc bus voltage controller for the GSC.

This PLL also has a module to extract the instantaneous positive and negative symmetrical components of the voltage of the microgrid [13]. The PLL was tuned based on its small signal analysis model for a bandwidth of 100 Hz. The block diagram of the current controller together with the filter (L<sub>f</sub>) model in a synchronous reference frame is illustrated in Fig. 8, where R<sub>f</sub> is the equivalent series resistance of the inductor L<sub>f</sub>, i<sub>e qs</sub> and i<sub>e ds</sub> are the currents in the delta side of transformer T<sub>2</sub>, and e<sub>qs</sub> and e<sub>ds</sub> are the dq-axis components of the microgrid voltage. The adopted current direction references are the same as those shown in Fig. 1. If the losses in the GSI and in the inductor L<sub>f</sub> are neglected, the variation of the energy stored in the capacitor C<sub>c</sub> is equal to the difference between the active power received from the microgrid (P<sub>s</sub>)

and the active power generated by the wind turbine (P<sub>g</sub>). Using the convention of Fig. 2, this can be expressed as in

$$\frac{1}{2} C_c \frac{dw_c}{dt} = P_s - P_g; w_c = v_c^2 \quad (2)$$

For a dq synchronous reference frame aligned with the microgrid voltage vector, it follows that e<sub>e ds</sub> = 0. Therefore, P<sub>s</sub> is equal to (3/2) E<sub>s</sub> i<sub>qs</sub>, with E<sub>s</sub> being the magnitude of the phase voltage, considered constant in this application. By defining K<sub>c</sub> equal to (3/2) E<sub>s</sub>, the dynamic equation for the capacitor C<sub>c</sub> is presented in

$$\frac{dw_c}{dt} = \frac{2}{C_c} (K_c i_{qs}^e - P_g) \quad (3)$$

The block diagram for the dc bus voltage controller is illustrated in Fig. 8. G<sub>DID3</sub> is the transfer function used to decouple the sample instants the effect of the disturbances due to P<sub>g</sub>, and τ<sub>f</sub> is the time constant L<sub>f</sub>/R<sub>f</sub>. The output of the voltage controller is the reference current (i<sub>e qs</sub>\*) for the inner current loop.

### V. PROPOSED STRATEGY TO CONTROL THE GENERATED POWER IN THE MICROGRID

In stand-alone and distributed renewable energy systems, there is no commercial or conventional grid to absorb any surplus power generated internally in the microgrid. Therefore, the generated power needs to be controlled when the load power is less than the amount of power that could be generated by the energy sources. This is necessary to keep the energy balance in the microgrid under control and to keep the battery bank voltage below or equal to its maximum allowable value. This is necessary since voltages higher than the gasification voltage can decrease the life span of batteries or even damage them irreversibly [17]. In the proposed control strategy, the GFC verifies the battery bank voltage to know if it reached the maximum allowed charging voltage and, if so, change the microgrid frequency to inform the other sources that they must reduce their generated power. Based on the microgrid frequency, the control systems of the power generation sources connected to the microgrid decide whether to restrict the power generated by each of them.

This control strategy can be explained based on Fig. 9. While the terminal voltage of the battery bank is below its maximum limit, the microgrid frequency (f) is determined according to the conventional droop control strategy, described by line C1 in Fig. 9, since a physical or virtual inductance is added when the line resistance cannot be neglected [7]. The frequency value is calculated by (8), where k<sub>p</sub> is the slope constant of the line C1. On this situation, there are no restrictions about the amount

of power that can be generated, and the existing renewable energysources can function on their maximum power point. Obviously, this is true only if the battery bank has been designed with sufficient capacity to absorb all the power that the renewablesources can produce at a given instant

$$f = f_0 - k_p P_{inv}$$

On the other hand, if the maximum voltage of the batterybank is reached, the microgrid frequency is imposed to be always higher than the value  $f_{max}$ , which is the maximum frequency of operation of the conventional droop control strategy. This is illustrated by the hatched area in Fig.9. Now, the value of the frequency ( $f$ ) is a variable that changes dynamically

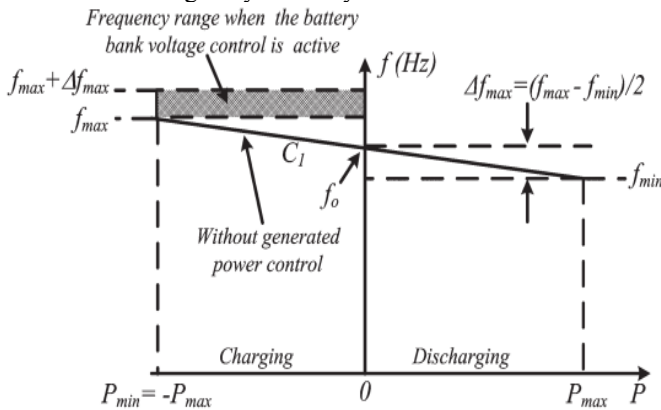


Fig. 9. Frequency versus power in the GFC based on the proposed power control.

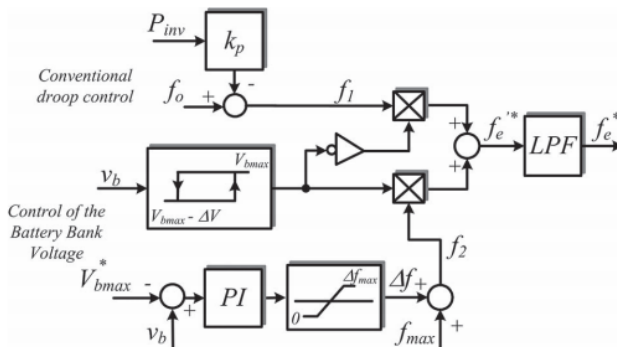


Fig. 10. Block diagram of the frequency control at the GFC.

With the terminal voltage of the battery bank ( $v_b$ ), the power generated internally in the microgrid ( $P_g$ ), and the power of the GFC ( $P_{inv}$ ). This can be expressed by (9). As the calculation of the frequency depends on the dynamics of the battery bank voltage controller, its relationship with the power ( $P_{inv}$ ) does not follow a well-defined algebraic equation as, for example, a straight line. Therefore, Fig. 3 shows only an illustration that the frequency can assume any value between  $f_{max}$  and  $f_{max} + \Delta f_{max}$ . In this operating condition, it is necessary to restrict the amount

of power that can be generated by renewable sources; otherwise, the integrity of the battery bank is at risk. The amount of power that needs to be reduced from the maximum power that each source is able to produce at every moment has a direct relation to the frequency difference  $\Delta f = f - f_{max}$ . The values of  $f_0$  and  $\pm \Delta f_{max}$  adopted in this work are 60 Hz and  $\pm 0.60$  Hz so that the frequency range of the microgrid is between 59.4 Hz ( $f_{min}$ ) and 61.2 Hz ( $f_{max} + \Delta f_{max}$ ).

$$f = f_{max} + \Delta f(v_b, P_g, P_{inv})$$

**A. Implementation of the Proposed Strategy in the GFC**

The control of the battery bank voltage, in order to ensure its integrity, was implemented as shown in Fig. 10. While the output of the hysteresis loop is zero, the value of the frequency reference is  $f_e^* = f_1$ . On the other hand, while the output of the hysteresis loop is one, a proportional and integral (PI) controller is used to regulate the terminal voltage of the battery bank equal or below its maximum allowed value ( $V_{bmax}$ ). The output of

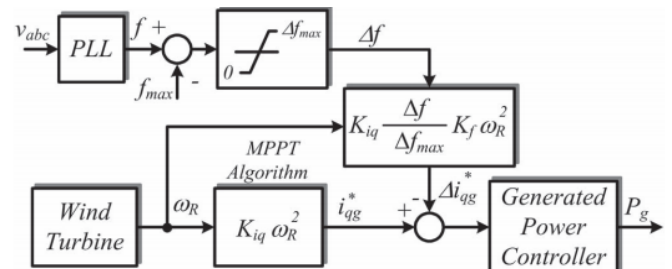


Fig. 11. Block diagram of the power control at the GSC.

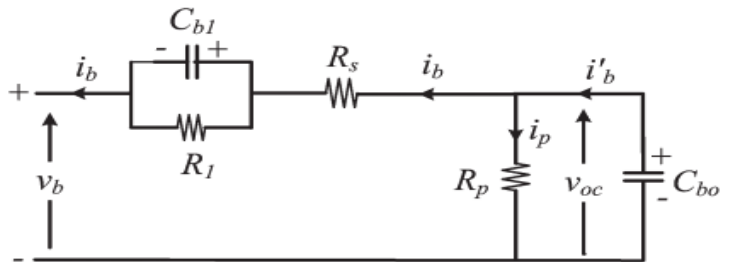


Fig. 12. Lead-acid battery equivalent circuit.

This controller is the increment of frequency ( $\Delta f$ ) that must be added to the value  $f_{max}$  to form the new microgrid frequency reference value ( $f_e^* = f_2 = f_{max} + \Delta f$ ). The value of  $\Delta f$  is proportional to the amount of power that must be decremented from the generated power in order to control the battery bank terminal voltage. The low-pass filter with a 1-Hz bandwidth shown in Fig. 9 is used to avoid sudden variations in frequency due to the hysteresis loop.

**B. Implementation of the Proposed Strategy in the GSC**

The grid frequency is measured by the GSC and if its value is higher than  $f_{max}$ , it means that the voltage of the battery bank is higher than its maximum allowed value. For the particular case where the renewable energy source is a wind turbine, the GSC power controller decrements the current reference  $i_q^*$ , originally calculated by (7), which is now calculated by (10), where  $K_f$  is a constant which serves to match the rated power of the GFC with the rated power of the wind turbine. The block diagram of this control action is presented in Fig. 11.

$$i_q^* = K_{iq} \left( 1 - \frac{\Delta f}{\Delta f_{max}} K_f \right) \omega_R^2$$

As the reference current is now determined by (10), the operating points of the wind turbine-generator set follow the dashed curve indicated by  $T_g$  in Fig. 8. This implies a reduction in the generator torque, which causes a reduction in power that is produced by the wind turbine keeping regulated the terminal voltage of the battery bank.

### C. Tuning of the Battery Bank Terminal Voltage Controller

The tuning of the PI controller shown in Fig. 10 takes into account the dynamic of the battery bank. One possible model for lead-acid batteries is shown in Fig. 12. In this figure,  $v_{oc}$  is the battery open circuit voltage,  $R_s$  is the equivalent series internal resistance,  $R_1$  and  $C_{b1}$  are used to model the over- or under voltage that happens when the battery is charging or discharging,  $R_p$  is the resistance due to the natural losses, and  $C_{bo}$  models the battery capacity to storage energy. Normally, the natural losses occur very slowly, so the effect of  $R_p$  can be disregarded for the purpose of this work.

## VI. INTRODUCTION TO FUZZY LOGIC CONTROLLER

L. A. Zadeh presented the first paper on fuzzy set theory in 1965. Since then, a new language was developed to describe the fuzzy properties of reality, which are very difficult and sometime even impossible to be described using conventional methods. Fuzzy set theory has been widely used in the control area with some application to dc-to-dc converter system. A simple fuzzy logic control is built up by a group of rules based on the human knowledge of system behavior. Matlab/Simulink simulation model is built to study the dynamic behavior of dc-to-dc converter and performance of proposed controllers. Furthermore, design of fuzzy logic controller can provide desirable both small signal and large signal dynamic performance at same time, which is not possible with linear control technique. Thus, fuzzy logic controller has been potential ability to improve the robustness of dc-to-dc converters. The basic scheme of a fuzzy logic

controller is shown in Fig 5 and consists of four principal components such as: a fuzzification interface, which converts input data into suitable linguistic values; a knowledge base, which consists of a data base with the necessary linguistic definitions and the control rule set; a decision-making logic which, simulating a human decision process, infer the fuzzy control action from the knowledge of the control rules and linguistic variable definitions; a de-fuzzification interface which yields non fuzzy control action from an inferred fuzzy control action [10].

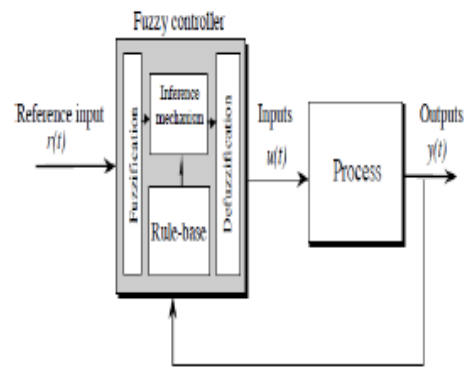


Fig.13. General Structure of the fuzzy logic controller on closed-loop system

The fuzzy control systems are based on expert knowledge that converts the human linguistic concepts into an automatic control strategy without any complicated mathematical model [10]. Simulation is performed in buck converter to verify the proposed fuzzy logic controllers.

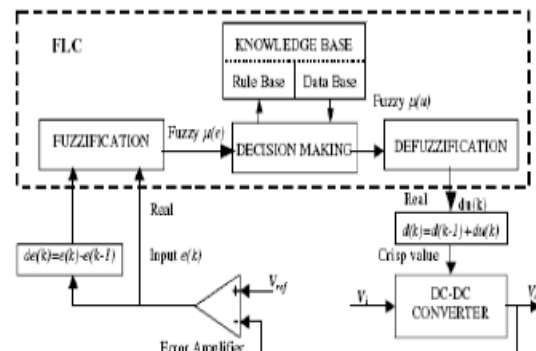
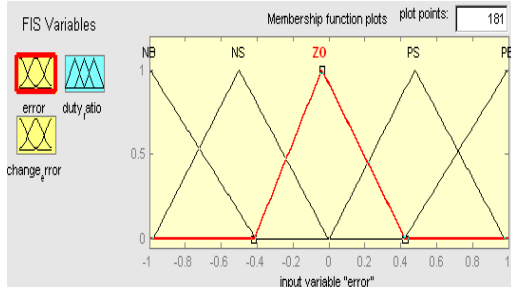


Fig.14. Block diagram of the Fuzzy Logic Controller (FLC) for dc-dc converters

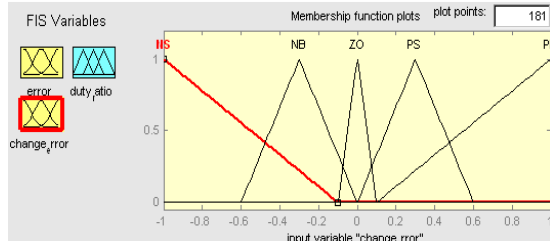
### A. Fuzzy Logic Membership Functions:

The dc-dc converter is a nonlinear function of the duty cycle because of the small signal model and its control method was applied to the control of boost converters. Fuzzy controllers do not require an exact mathematical model. Instead, they are designed based on general

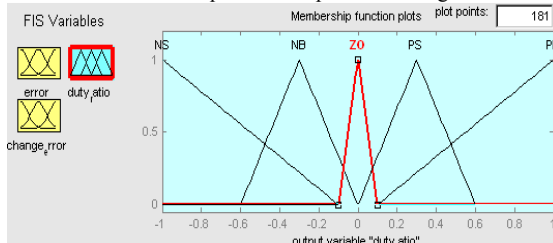
knowledge of the plant. Fuzzy controllers are designed to adapt to varying operating points. Fuzzy Logic Controller is designed to control the output of boost dc-dc converter using Mamdani style fuzzy inference system. Two input variables, error (e) and change of error (de) are used in this fuzzy logic system. The single output variable (u) is duty cycle of PWM output.



The Membership Function plots of error



The Membership Function plots of change error



The Membership Function plots of duty ratio

### B. Fuzzy Logic Rules:

The objective of this dissertation is to control the output voltage of the boost converter. The error and change of error of the output voltage will be the inputs of fuzzy logic controller. These 2 inputs are divided into five groups; NB: Negative Big, NS: Negative Small, ZO: Zero Area, PS: Positive small and PB: Positive Big and its parameter [10]. These fuzzy control rules for error and change of error can be referred in the table that is shown in Table II as per below:

Table II: Rules for error and change of error

(de) \ (e)	NB	NS	ZO	PS	PB
NB	NB	NB	NB	NS	ZO
NS	NB	NB	NS	ZO	PS
ZO	NB	NS	ZO	PS	PB
PS	NS	ZO	PS	PB	PB
PB	ZO	PS	PB	PB	PB

## VII MATLAB/SIMULATION RESULTS

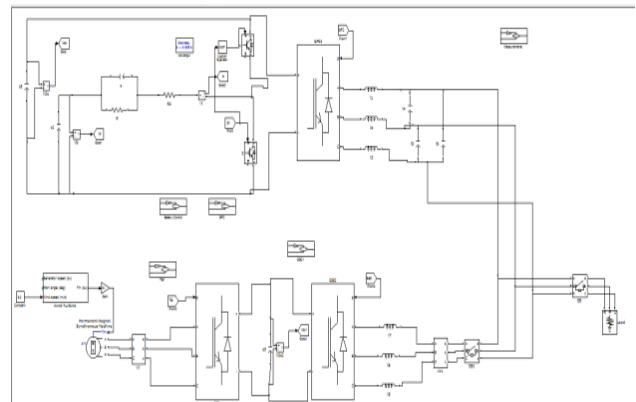


Fig 15 Matlab/simulation circuit of Simplified diagram of the studied microgrid.

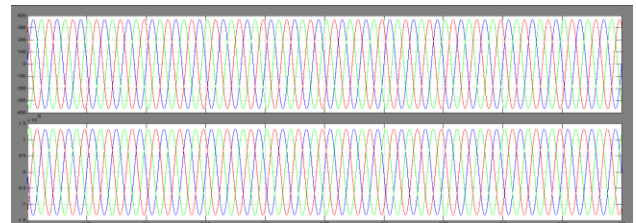


Fig 16 simulation wave form of grid voltage and current

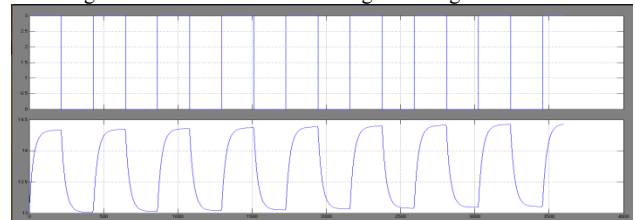
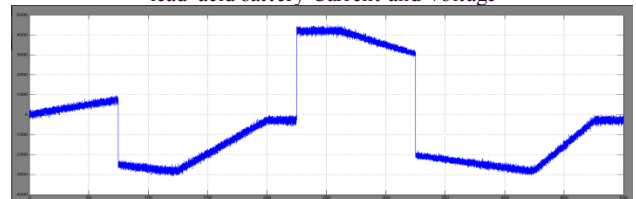


Fig 17 simulation wave form of during the tests with a 30-Ah 12-V lead-acid battery Current and Voltage



(a)

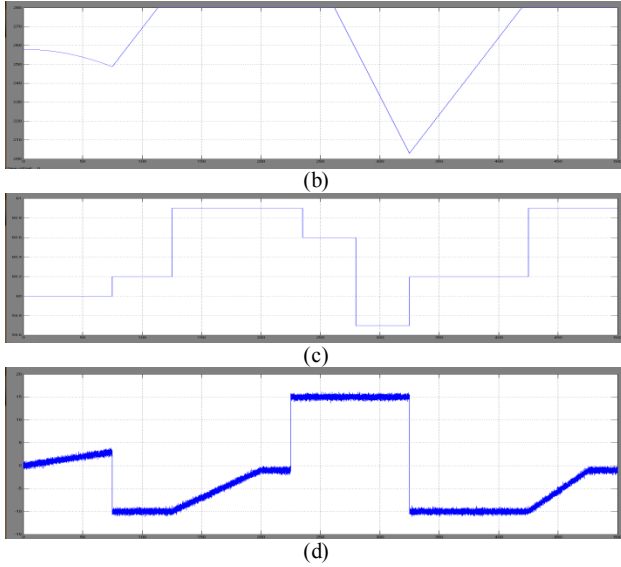


Fig 18 simulation wave form of Operation with a constant wind speed of 9.2 m/s: (a) Power at the GFC terminals, (b) battery bank voltage, (c) microgrid frequency, and (d) battery current

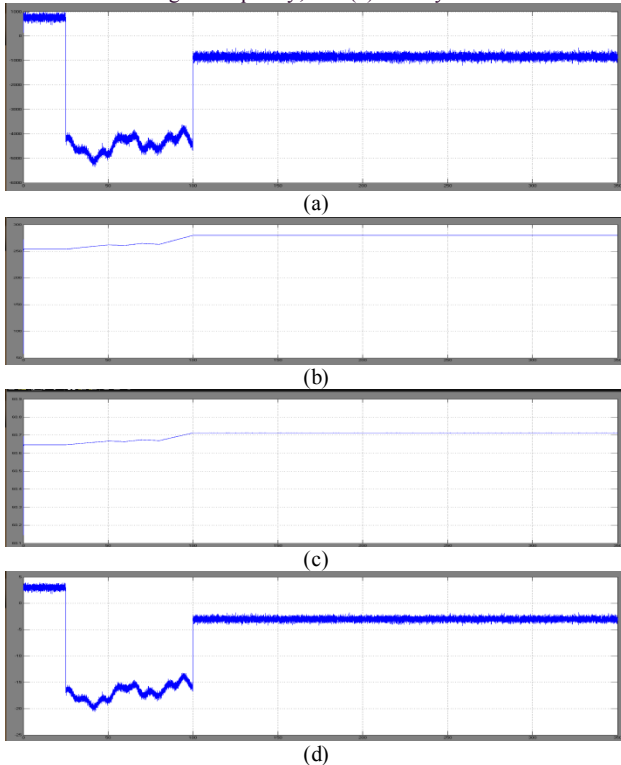


Fig 19 simulation wave form of operation with variable wind speed: (a) Power at the GFC terminals, (b) battery bank voltage, (c) microgrid frequency, and (d) battery current.

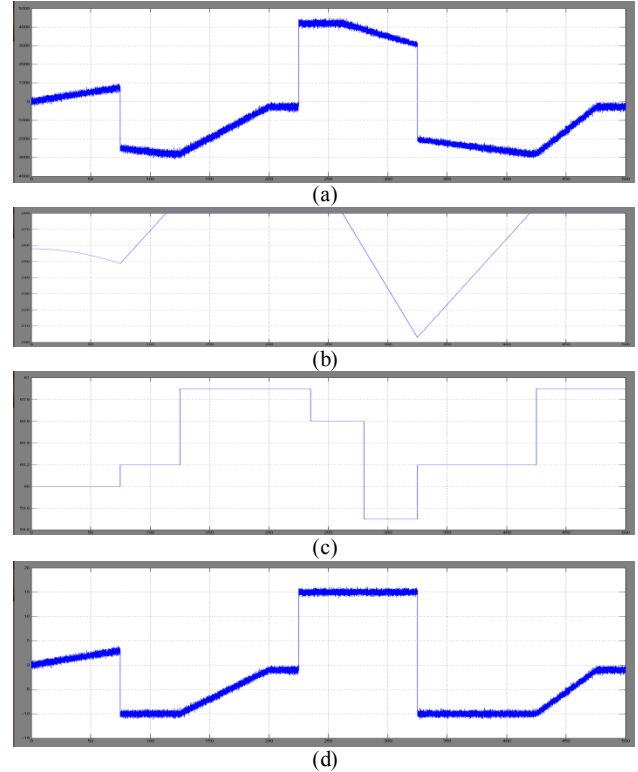


Fig 20 simulation wave form of operation with variable wind speed with fuzzy controller : (a) Power at the GFC terminals, (b) battery bank voltage, (c) microgrid frequency, and (d) battery current

## VIII CONCLUSION

This paper proposed controller is a strategy to fuzzy logic control the generated power in order to keep the charging voltage battery banks under control in stand-alone microgrid with distributed renewable energy sources. This strategy does not need wired communication between the distributed renewable sources nor dump loads to dissipate the surplus of generated power in the microgrid. These technical advantages make the proposed strategy a promising tool to increase the viability and reliability of the renewable power generation system installed in isolated and remote communities. Although a wind turbine has been used to demonstrate the validity of the proposed strategy, it is also valid regardless of the power source existing in the isolated microgrid. The proposed strategy calculates the amount of power that must be generated at each time by each source in order to keep the balance of energy into the microgrid. In other words, the sum of the generated, consumed, and stored energy must always be zero all the time





## REFERENCES

- [1] José G. de Matos, Member, IEEE, Felipe S. F. e Silva, Student Member, IEEE, and Luiz A. de S. Ribeiro, Member, IEEE, "Power Control in AC Isolated Micro grids With Renewable Energy Sources and Energy Storage Systems" *IEEE Transactions On Industrial Electronics*, Vol. 62, No. 6, June 2015.
- [2] L. A. de S. Ribeiro, O. R. Saavedra, S. L. de Lima, and J. G. de Matos, "Isolated micro-grid with renewable hybrid generation: The case of Lençóis island," *IEEE Trans. Sustain. Energy*, vol. 2, no. 1, pp. 1–11, Jan. 2011.
- [3] L. A. de S. Ribeiro, O. R. Saavedra, S. L. de Lima, and J. G. de Matos, "Making isolated renewable energy systems more reliable," *Renew. Energy*, vol. 45, pp. 221–231, Sep. 2012.
- [4] J. G. de Matos, L. A. de S. Ribeiro, and E. C. Gomes, "Power control in ac autonomous and isolated micro grids with renewable energy sources and energy storage systems," in *Proc. IEEE IECON*, 2013, pp. 1827–1832.
- [5] N. Mendis, K. M. Muttaqi, S. Pereira, and M. N. Uddin, "A novel control strategy for stand-alone operation of a wind dominated RAPS system," in *Proc. IEEE IAS Annu. Meeting*, 2011, pp. 1–8.
- [6] J. Chen, J. Cheng, C. Gong, and X. Deng, "Energy management and power control for a stand-alone wind energy conversion system," in *Proc. IEEE IECON*, 2012, pp. 989–994.
- [7] M. J. Erickson and R. H. Lasseter, "Integration of battery storage element in a CERTS microgrid," in *Proc. IEEE ECCE*, 2010, pp. 2570–2577.
- [8] J. Rocabert, J. A. Luna, F. Blaabjerg, and P. Rodríguez, "Control of power converters in ac microgrids," *IEEE Trans. Power Electron.*, vol. 27, no. 11, pp. 4734–4749, Nov. 2012.
- [9] C. Jin, P. Wang, J. Xiao, Y. Tang, and F. H. Choo, "Implementation of hierarchical control in dc microgrids," *IEEE Trans. Ind. Electron.*, vol. 61, no. 8, pp. 4032–4042, Feb. 2014.
- [10] X. Lu, K. Sun, J. M. Guerrero, J. C. Vasquez, and L. Huang, "State-of-charge balance using adaptive droop control for distributed energy storage systems in dc microgrid applications," *IEEE Trans. Ind. Electron.*, vol. 61, no. 6, pp. 2804–2815, Jun. 2014.
- [11] M. A. Abusara, J. M. Guerrero, and S. M. Sharkh, "Line-interactive UPS for microgrids," *IEEE Trans. Ind. Electron.*, vol. 61, no. 3, pp. 1292–1300, Mar. 2014.
- [12] J. M. Guerrero, P. X. Loh, T.-L. Lee, and M. Chandorkar, "Advanced control architectures for intelligent micro grids—Part II: Power quality, energy storage, ac/dc microgrids," *IEEE Trans. Ind. Electron.*, vol. 60, no. 4, pp. 1263–1270, Apr. 2013.
- [13] Z. Chen, J. M. Guerrero, and F. Blaabjerg, "A review of the state of art of power electronics for wind turbines," *IEEE Trans. Power Electron.*, vol. 24, no. 8, pp. 1859–1875, Aug. 2009.